JOURNAL OF COMPUTATIONAL PHYSICS 115, 169–183 (1994)

Grid Adaption Based on Modified Anisotropic Diffusion Equations Formulated in the Parametric Domain*

R. HAGMEIJER

Fluid Dynamics Division, Theoretical Aerodynamics Department, National Aerospace Laboratory (NLR), The Netherlands

Received July 20, 1992; revised March 28, 1994

A new grid-adaption algorithm for problems in computational fluid dynamics is presented. The basic equations are derived from a variational problem formulated in the parametric domain of the mapping that defines the existing grid. Modification of the basic equations provides desirable properties in boundary layers. The resulting modified anisotropic diffusion equations are solved for the computational coordinates as functions of the parametric coordinates and these functions are numerically inverted. Numerical examples show that the algorithm is robust, that shocks and boundary layers are well-resolved on the adapted grid, and that the flow solution becomes a globally smooth function of the computational coordinates.

1. INTRODUCTION

A major problem within the field of computational fluid dynamics (CFD) is the generation of appropriate structured computational grids such that sufficient accuracy of the numerical flow solution is obtained with a limited number of grid points. The required density of grid points is determined in general by gradients, such as gradients of the flow solution and curvature of the geometry. Large gradients require a high grid-point density in order to reduce the numerical errors. At the stage of grid generation the flow solution is unknown, however, and the prescription of grid resolution has to be based on a qualitative estimate of the flow solution.

To eliminate the need for a priori qualitative estimates of the flow solution, considerable effort has been directed towards the development of solution-adaptive grid generation methods; see, e.g., the surveys of Eiseman [1] and Thompson [2]. In general these methods redistribute the points of a structured grid with the objective to improve accuracy of the flow solution by recalculation of the flow on the adapted grid. Many of the methods reviewed in [1, 2] are related to the one-dimensional equidistribution principle which requires grid spacing to be inversely proportional to a weight function. The weight function is commonly taken as some norm of the first and/or second derivatives of the flow solution. The equidistribution principle can be formulated in a number of different ways [1] such as the variational statement and the differential statement formed by the Euler equation of the variational statement.

Numerous researchers have developed extensions of the one-dimensional equidistribution principle into two or three dimensions. Dwyer [3] successfully applied equidistribution along one family of grid lines (arcs in physical space along which one of the computational coordinates is a constant) within two-dimensional problems. Nakahashi and Deiwert [4] applied the concept of equidistribution along both families of grid lines but added orthogonality control by means of a torsion spring analogy to prevent the occurrence of cells with excessive skewness. Anderson and Steinbrenner [5] and Anderson [6] noted that the Thompson non-adaptive grid generation scheme based upon solving a system of Poisson equations [7], can be interpreted as an equidistribution of curvature and orthogonality along grid lines. Comparison with the one-dimensional equidistribution principle led them to express the source terms in the Poisson equations in terms of weight functions that measure the flow solution activity along grid lines. Anderson [8] exploited the diffusive form of the Poisson equations suggested by Winslow [9] and expressed the diffusion coefficient in terms of a single weight function. This method can be interpreted as an equidistribution scheme where the product of a weight function and cell area/volume is equidistributed over the physical domain. Winslow [9] showed that the diffusion equations are the Euler equations of a variational problem formulation.

The present paper describes an extension of the one-dimensional variational equidistribution statement into two dimensions which can be directly extended into three dimensions. Separate weight functions are used in the func-

* This investigation has partly been carried out under a contract awarded by the European Economic Community within the BRITE/EURAM 1042 EUROMESH project, Contract Number AERO.0018.C(H).

0021-9991/94 $6.00

tional while the resulting Euler equations are linear and uncoupled partial differential equations. Similar to the work of Lee and Loellbach [10] the equations are formulated in the so-called parametric domain to retain the global characteristics of the initial grid. To prevent the occurrence of skew cells in boundary layers, the adaption equations are slightly modified. Finally numerical adaption examples are presented.

2. ADAPTIVE GRID GENERATION IN THE PARAMETRIC DOMAIN

Let $\Omega \subset \mathbb{R}^2$ be the physical domain in two-dimensional space on which a computational grid has to be adapted, and let $\Omega_c = [0, 1]^2 \subset \mathbb{R}^2$ be the so-called computational domain. A boundary-conforming curvilinear coordinate system in Ω can be defined by mapping Ω_c onto Ω, so that the cartesian computational coordinates $\xi = (\xi, \eta)^T$ in Ω_c are the curvilinear coordinates in Ω and are mapped onto the physical coordinates $\mathbf{x} = (x, y)^T$ in Ω. The problem of grid generation in general and grid adaption in particular can be formulated in terms of the determination of a suitable mapping from Ω_c to Ω. In the present paper it is assumed that the initial grid incorporates sufficient quality w.r.t. geometry resolution, orthogonality, and smoothness and has merely to be adapted to the flow solution. To retain the characteristics of the initial grid in a global way, the adaption equations are formulated in the parametric domain, based on the idea of Lee and Loellbach [10]. The concept of grid adaption in the parametric domain is illustrated in Fig. 1. Let the initial grid in the physical domain Ω be the image of a uniform cartesian grid in the unit square $[0, 1]^2 \subset \mathbb{R}^2$ under a mapping M. The cartesian coordinates in the unit square denoted by $\mathbf{p} = (p, q)^T$ serve as parameters to describe the physical domain; hence the unit square is called the parametric domain, denoted in the present paper by Ω_p. The idea is to adapt the cartesian grid in Ω_p and to apply the mapping M to generate the adapted grid in Ω.

An attractive feature of grid adaption in the parametric domain is the natural retainment of global characteristics of the initial grid in the physical domain, such as high resolution at geometry parts with high curvature. Hence, the initial grid can be considered to be adapted to the geometry, whereas the regenerated grid is additionally adapted to the flow solution.

The problem of grid adaption in Ω_p can conveniently be formulated in terms of determination of a suitable mapping A that maps a cartesian grid in the computational domain Ω_c to the adapted grid in Ω_p (see Fig. 1). Consequently, the adapted grid in the physical domain Ω is the image of the cartesian grid in Ω_c produced by the compound mapping $M \circ A$. Hence the problem is to find the parametric coordinates p and q as functions of the computational coordinates ξ and η, which is the main topic of the next sections.

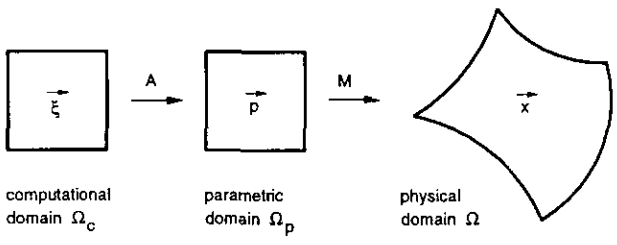

FIG. 1. Grid adaption by using an adaptive mapping A that maps the computational domain onto the parametric domain.

3. BASIC ADAPTION MAPPING

In one-dimensional adaption problems the mapping between the computational domain $[0, 1] \subset \mathbb{R}$ and the parametric domain $[0, 1] \subset \mathbb{R}$ can be defined as the solution of the one-dimensional equidistribution statement. In differential form the statement can be written as:

$$\frac{d}{dp}\left(\frac{\xi_p}{w}\right) = 0, \qquad p(0) = 0, \qquad p(1) = 1, \tag{1}$$

where $w(p)$ is a positive weight function that measures the flow activity in some sense. From (1) it directly follows that

$$\frac{1}{w}\xi_p = \text{const} \Rightarrow w p_\xi = \text{const},$$

resulting in small values of p_ξ when w is large and vice versa. Since w is a measure of flow activity in Ω_p and p_ξ is a measure of grid spacing in Ω_p, the grid is dense where flow activity is high and the grid is sparse where flow activity is low. Equation (1) is the Euler equation associated with a variational formulation of the equidistribution statement, which minimizes the functional

$$I[\xi] = \int_0^1 \frac{\xi_p^2}{w}\, dp. \tag{2}$$

The variational formulation (2) of the one-dimensional equidistribution statement is taken in this paper as a starting-point for the extension into multiple dimensions. Only the two-dimensional case is discussed, but all developments can directly be extended into three dimensions.

A generic extension of the functional (2) suitable for two-dimensional problems is

$$K[\xi(\mathbf{p})] = \iint_{\Omega_p} \left(\frac{\xi_p^2}{w_{11}} + \frac{\xi_q^2}{w_{12}} + \frac{\eta_p^2}{w_{21}} + \frac{\eta_q^2}{w_{22}}\right) dp\, dq, \tag{3}$$

where the weight functions w_{ij} are bounded differentiable functions of $\mathbf{p}$ satisfying

$$w_{ij} \geq C \qquad \text{for all } i, j,$$

with the constant C conviently taken $C = 1$. It should be noted that for general functions w_{ij} the functional (3) is not a member of the two classes of functionals evaluated by Warsi and Thompson [12], since the integrand of (3) cannot be expressed in terms of the metric coefficients.

A necessary condition for the functional K to become stationary is that its integrand satisfy the Euler equations

$$\frac{\partial}{\partial p}\left(\frac{\xi_p}{w_{11}}\right)+\frac{\partial}{\partial q}\left(\frac{\xi_q}{w_{12}}\right)=0, \tag{4a}$$

$$\frac{\partial}{\partial p}\left(\frac{\eta_p}{w_{21}}\right)+\frac{\partial}{\partial q}\left(\frac{\eta_q}{w_{22}}\right)=0, \tag{4b}$$

which are linear and decoupled partial differential equations for the functions $\xi(\mathbf{p})$ and $\eta(\mathbf{p})$, respectively. A number of grid generation equations that have been reported in the literature can be extracted from the generic model (3) and (4) if p and q are replaced by x and y. First, if all weight functions are constant, i.e., $w_{ij} \equiv 1$ for $i = 1, 2$ and $j = 1, 2$ then K is identical to the smoothness integral of Brackbill and Saltzmann [11] and the Euler equations (4) return to the Laplace equations, which can be used to some extent for non-adaptive grid generation.

Second, if all weight functions are identical, i.e., $w_{ij} \equiv w$ for $i = 1, 2$ and $j = 1, 2$, then K is identical to the functional used by Winslow [9] and the Euler equations become two identical isotropic diffusion equations for $\xi(\mathbf{p})$ and $\eta(\mathbf{p})$, which have been applied by Anderson [8]. Although these equations enable grid adaption, the use of a single weight function does not allow for anisotropic adaption in the direction of the flow solution gradients which is required in realistic CFD problems.

Finally, if two separate weight functions are used, i.e., $w_{11} \equiv w_{12} \equiv w_1$ and $w_{21} \equiv w_{22} \equiv w_2$, then K is identical to the integral proposed by Eiseman [1] and the Euler equations (4) become two distinct isotropic diffusion equations for $\xi(\mathbf{p})$ and $\eta(\mathbf{p})$ which allow for anisotropic adaption. However, since w_1 and w_2 weight the gradients of ξ and η, respectively, flow derivatives in the directions of these gradients must be explicitly incorporated in order to obtain anisotropic adaption. Hence the weight functions will depend on the mapping $\boldsymbol{\xi}(\mathbf{p})$ such that Eqs. (4) are not the correct Euler equations for the functional K, see Warsi and Thompson [12]. Anderson and Steinbrenner [5, 6] apply these equations with the exception of some terms. Alternatively Kim and Thompson [13] propose to use gradients of separate flow solution components in the weight functions (e.g., pressure in w_1 and velocity in w_2). Although derivatives are taken w.r.t. p and q (or x and y) such that Eqs. (4) are indeed the correct Euler equations, there is a risk that the p and q (or x and y) coordinate lines are not aligned with the gradients of ξ and η, respectively.

In order to enable anisotropic adaption based on the Euler equations (4) with two weight functions that are associated with flow solution derivatives w.r.t. p and q instead of ξ and η, it is proposed to take $w_{11} \equiv w_{21} \equiv w_1$ and $w_{12} \equiv w_{22} \equiv w_2$ for which the functional K can be written as

$$K[\boldsymbol{\xi}(\mathbf{p})] = \iint_{\Omega_p} \left(\frac{\|\boldsymbol{\xi}_p\|^2}{w_1}+\frac{\|\boldsymbol{\xi}_q\|^2}{w_2}\right) dp\, dq. \tag{5}$$

In contrast to the integral described by Eiseman [1] with the integrand incorporating normals along curves in the parametric domain of constant ξ or η, the present integral is expressed in terms of tangents along curves in the computational domain of constant q or p. Hence it is natural to associate w_1 and w_2 with derivatives of the flow solution w.r.t. p and q, respectively. The resulting Euler equations become two identical anisotropic diffusion equations for $\xi(p, q)$ and $\eta(p, q)$,

$$\frac{\partial}{\partial p}\left(\frac{\xi_p}{w_1}\right)+\frac{\partial}{\partial q}\left(\frac{\xi_q}{w_2}\right)=0, \tag{6a}$$

$$\frac{\partial}{\partial p}\left(\frac{\eta_p}{w_1}\right)+\frac{\partial}{\partial q}\left(\frac{\eta_q}{w_2}\right)=0, \tag{6b}$$

which form the basis for specification of the inverse adaption mapping A^{-1} in Fig. 1.

The requirement that the adapted grid in the parametric domain Ω_p given by the functions $p(\xi, \eta)$ and $q(\xi, \eta)$ be boundary conforming leads to the boundary conditions

$$\xi(0, q) = 0, \quad \xi(1, q) = 1, \quad \eta(p, 0) = 0, \quad \eta(p, 1) = 1. \tag{7}$$

In addition, if no further conditions are specified, a set of natural boundary conditions has to be satisfied in order to make the functional K stationary (Ref. [14]):

$$\begin{aligned} \xi_q(p, 0) &= 0, \qquad \xi_q(p, 1) = 0, \\ \eta_p(0, q) &= 0, \qquad \eta_p(1, q) = 0. \end{aligned} \tag{8}$$

It should be noted, however, that the Neumann boundary conditions (8) may partly or entirely be replaced by Dirichlet boundary conditions.

The stationary point of K is indeed a minimum. To show this, let a function Φ be defined as

$$\Phi(\varepsilon_1, \varepsilon_2) \equiv K[\xi + \varepsilon_1 \tilde{\xi}, \eta + \varepsilon_2 \tilde{\eta}],$$

with $\tilde{\xi}$ and $\tilde{\eta}$ being admissible perturbation functions of the

solution $\xi = (\xi, \eta)^T$, and with ε_1 and ε_2 as arbitrary real valued constants. Taylor expansion of Φ around $\varepsilon_1 = \varepsilon_2 = 0$, with $\partial\Phi/\partial\varepsilon_1 = \partial\Phi/\partial\varepsilon_2 = 0$ due to the Euler equations (6) and conditions (7), (8), yields

$$\Phi(\varepsilon_1, \varepsilon_2) - \Phi(0, 0) \equiv \frac{1}{2}\varepsilon_1^2 \frac{\partial^2\Phi}{\partial\varepsilon_1^2} + \frac{1}{2}\varepsilon_2^2 \frac{\partial^2\Phi}{\partial\varepsilon_2^2},$$

with

$$\frac{\partial^2\Phi}{\partial\varepsilon_1^2} = 2\iint_{\Omega_p} \left(\frac{\tilde{\xi}_p^2}{w_1} + \frac{\tilde{\xi}_q^2}{w_2}\right) dp\, dq,$$

$$\frac{\partial^2\Phi}{\partial\varepsilon_2^2} = 2\iint_{\Omega_p} \left(\frac{\tilde{\eta}_p^2}{w_1} + \frac{\tilde{\eta}_q^2}{w_2}\right) dp\, dq.$$

Hence it follows that $\Phi(\varepsilon_1, \varepsilon_2) - \Phi(0, 0) \geqslant 0$ with equality if and only if $\varepsilon_1 = \varepsilon_2 = 0$, which proves the assertion.

Finally it is interesting to note that, upon integration of Eq. (6a) w.r.t. q, integration of Eq. (6b) w.r.t. p, and application of the natural boundary conditions (8), the following two equations hold:

$$\frac{\partial}{\partial p}\int_0^1 \frac{\xi_p}{w_1}\, dq = 0, \qquad \frac{\partial}{\partial q}\int_0^1 \frac{\eta_q}{w_2}\, dp = 0.$$

These expressions can be interpreted as averaged forms of the one-dimensional equidistribution statement (1).

4. MODIFICATION OF THE ADAPTION MAPPING

A disadvantage of grid adaption in the parametric domain is the possible generation of excessive skew cells in the physical domain when the initial grid incorporates cells with aspect ratios that are much larger or smaller than unity. To illustrate this, let ϕ be the angle between two lines of the adapted grid in Ω with constant ξ and η, respectively, and let the initial grid in Ω be orthogonal:

$$\mathbf{x}_p \cdot \mathbf{x}_q = 0.$$

The angle ϕ can be expressed as

$$\phi = \arccos\left(\frac{\mathbf{x}_\xi \cdot \mathbf{x}_\eta}{\|\mathbf{x}_\xi\|\, \|\mathbf{x}_\eta\|}\right),$$

which upon substitution of the functions $p(\xi, \eta)$ and $q(\xi, \eta)$ can be written as

$$\phi = \arccos\left(\frac{p_\xi p_\eta + \alpha^2 q_\xi q_\eta}{\sqrt{p_\xi^2 + \alpha^2 q_\xi^2}\sqrt{p_\eta^2 + \alpha^2 q_\eta^2}}\right), \tag{9}$$

where α is the local cell aspect ratio of the initial grid:

$$\alpha = \|\mathbf{x}_q\|/\|\mathbf{x}_p\|.$$

From (9) it can be deduced that when the adapted grid in the parametric domain is nearly orthogonal, i.e.,

$$\mathbf{p}_\xi \cdot \mathbf{p}_\eta = p_\xi p_\eta + q_\xi q_\eta \ll \sqrt{p_\xi^2 + q_\xi^2}\sqrt{p_\eta^2 + q_\eta^2} = \|\mathbf{p}_\xi\|\, \|\mathbf{p}_\eta\|,$$

the adapted grid in Ω is also nearly orthogonal when $\alpha \approx 1$. However, when $\alpha \ll 1$ or $\alpha \gg 1$ Eq. (9) shows that $\phi \sim 0$ when $p_\xi p_\eta \neq 0$ or $q_\varepsilon q_\eta \neq 0$, respectively; i.e., the adapted grid in Ω is collapsed. Cells of large or small aspect ratios within the field of CFD occur commonly in boundary layers. Most Navier–Stokes solvers need orthogonal grids in boundary layers; i.e., grid lines are required to originate from solid surfaces in the normal direction. Moreover, gradients in the normal direction are much larger than in the tangential direction. Hence it is desirable that the grid in the boundary layers is primarily adapted in the normal direction and that the adaption in the tangential direction is constrained by the orthogonality requirement. To obtain this property of the adaption algorithm, the adaption equations (6) are modified,

$$\lambda_1 \frac{\partial}{\partial p}\left(\frac{\xi_p}{w_1}\right) + \lambda_2 \frac{\partial}{\partial q}\left(\frac{\xi_q}{w_2}\right) = 0, \tag{10a}$$

$$\lambda_1 \frac{\partial}{\partial p}\left(\frac{\eta_p}{w_1}\right) + \lambda_2 \frac{\partial}{\partial q}\left(\frac{\eta_q}{w_2}\right) = 0, \tag{10b}$$

where λ_1 and λ_2 are functions of p and q which are taken proportionally to the squares of the local spacings of the initial grid in Ω:

$$\lambda_1 \sim \|\mathbf{x}_q\|^2, \qquad \lambda_2 \sim \|\mathbf{x}_p\|^2.$$

With this choice the ratio λ_1/λ_2 is proportional to the square of the cell aspect ratio:

$$\lambda_1/\lambda_2 \sim \alpha^2.$$

To illustrate the effect of the modification functions λ_1 and λ_2 let the edge $q = 0$ in Ω_p represent a solid wall in Ω and let the cells of the initial grid along the wall be orthogonal and have very small aspect ratios, i.e., $\alpha \ll 1$. As a consequence $\lambda_1 \ll \lambda_2$ and the modified equations can be approximated as

$$\frac{\partial}{\partial q}\left(\frac{1}{w_2}\xi_q\right) \approx 0, \qquad \frac{\partial}{\partial q}\left(\frac{1}{w_2}\eta_q\right) \approx 0. \tag{11}$$

Suppose that the Neumann boundary conditions (8) are applied, then $\xi_q(p, 0) = 0$ and consequently $\xi_q = 0$ for increasing q as long as the approximation (11) is valid, i.e.,

as long as $\lambda_1 \ll \lambda_2$. Hence the adapted grid in the boundary layer is nearly orthogonal. A second implication of the approximation (11) is that the equation for η (the second equation of (11)) is similar to Eq. (1) which shows that the grid in the boundary layer is adapted in the normal direction by one-dimensional equidistribution of the product $w_2^{-1}\eta_q$.

Finally the boundary value problems based on the modified adaption equations for the functions $\xi(p, q)$ and $\eta(p, q)$ can be conveniently formulated by means of a linear differential operator L_p defined as

$$L_p \equiv \Lambda \nabla_p \cdot W^{-1} \nabla_p, \tag{12}$$

where ∇_p is the Nabla operator $(\partial/\partial p, \partial/\partial q)^T$ and Λ and W are diagonal matrices:

$$\Lambda = \begin{pmatrix} \lambda_1 & 0 \\ 0 & \lambda_2 \end{pmatrix}, \qquad W = \begin{pmatrix} w_1 & 0 \\ 0 & w_2 \end{pmatrix}. \tag{13}$$

With the operator L_p the two boundary value problems for ξ and η are formulated as:

$$\begin{aligned} &L_p[\xi] = 0, \qquad (p, q)^T \in \Omega_p, \\ &\xi(0, q) = 0, \qquad \xi(1, q) = 1, \\ &\xi_q(p, 0) = \xi_q(p, 1) = 0, \end{aligned} \tag{14}$$

and

$$\begin{aligned} &L_p[\eta] = 0, \qquad (p, q)^T \in \Omega_p, \\ &\eta_p(0, q) = \eta_p(1, q) = 0, \\ &\eta(p, 0) = 0, \qquad \eta(p, 1) = 1. \end{aligned} \tag{15}$$

The weight functions w_1 and w_2 in (13) are specified in the next section.

5. WEIGHT FUNCTIONS

In this section the weight functions w_1 and w_2 that control the linear differential operator L_p defined by Eqs. (12) and (13) are specified. Two questions are of importance:

(i) in what way can the weight functions be chosen such that the accuracy of the numerical flow solution is improved upon recalculation on the adapted grid, and

(ii) in what way is the specification of the weight functions influenced by the fact that the adaption problem is formulated in the parametric domain.

Both questions can be analyzed to some extent for one-dimensional problems with the flow solution characterized by a single scalar function.

Let $Q \in \mathbb{R}$ be a scalar function of $x \in [0, L] \subset \mathbb{R}$ that represents a flow solution in one space dimension in the physical domain, and let the adapted computational grid be determined by the one-dimensional equidistribution statement (1), formulated in the physical domain, which can be written as

$$\xi_x = cw, \qquad c^{-1} = \int_0^L w\, dx,$$

where c is an integration constant. It is assumed that discretizations of the flow equations are second-order accurate in space and incorporate numerical truncation errors that are proportional to the second derivative of the flow solution in the computational domain.

Hence it is important to analyze the effect of grid adaption on the second derivative $Q_{\xi\xi}$. Let the weight function w be a positive function of x which ensures that $\xi_x > 0$. With $Q_x = Q_\xi \xi_x$ and $Q_{xx} = Q_{\xi\xi}\xi_x^2 + Q_\xi \xi_{xx}$, it is possible to express $Q_{\xi\xi}$ as

$$Q_{\xi\xi} = \frac{1}{c^2 w^2}\left(Q_{xx} - \frac{w_x}{w} Q_x\right).$$

Hence when Q_x is positive for all $x \in [0, L]$, the second derivative $Q_{\xi\xi}$ is identically zero if the weight function is taken as $w = Q_x$, which eliminates the leading term in the truncation error of the discrete approximation of Q. An equivalent equidistribution statement can be formulated in the parametric domain by substitution of $\xi_x = \xi_p p_x$, $Q_x = Q_p p_x$ and dividing by p_x:

$$\xi_p = cw^*, \qquad w^* = Q_p.$$

Hence in the particular case of positive Q_x and taking $w = Q_x$ and $w^* = Q_p$, formulation in the parametric domain is not only equivalent but also similar to formulation in the physical domain. In practice, however, it is not possible to take $w^* = Q_p$, since this leads to infinite grid spacing when $Q_p = 0$.

As an alternative, the equidistribution statement is modified to

$$\xi_p = cw^*, \qquad w^* = \sqrt{1 + Q_p^2}.$$

Consequently $w^* = 1$ when $Q_p = 0$ but $w^* \to |Q_p|$ when $Q_p^2 \gg 1$. The equivalent statement formulated in the physical domain is not similar anymore:

$$\xi_x = cw, \qquad w = \sqrt{p_x^2 + Q_x^2}.$$

When the flow solution is uniform, e.g., $Q_x \equiv 0$, the weight function w is equal to p_x and the initial grid is retained. This

is in contrast with the situation that the equidistribution statement is directly formulated in the physical domain with p_x^2 in w replaced by unity, which results in a uniform grid when $Q_x \equiv 0$.

The above presented analysis of one-dimensional problems with the flow solution represented by a single scalar function can be used as a guide for an extension to two-dimensional problems with the flow solution represented by a vector function. Hence the weight functions w_1 and w_2 that determine the operator L_p are chosen as

$$w_1 = \sqrt{1 + \|\mathbf{Q}_p\|^2}, \qquad w_2 = \sqrt{1 + \|\mathbf{Q}_q\|^2}, \tag{16}$$

where $\mathbf{Q} \in \mathbb{R}^n$ represents the flow solution with all the components scaled to $O(1)$ and $\|\cdot\|$ denotes the L_2-norm.

Taking w_1 and w_2 according to Eqs. (16) yields that, in the case that the flow solution $\mathbf{Q}$ is a bilinear function of p and q, i.e.,

$$\mathbf{Q}_{pp} = 0 \qquad \text{and} \qquad \mathbf{Q}_{qq} = 0,$$

then the initial grid is optimal in the sense that discretisation errors will be relatively small. Since the weight functions satisfy

$$\frac{\partial w_1}{\partial p} = 0 \qquad \text{and} \qquad \frac{\partial w_2}{\partial q} = 0,$$

the trivial solutions $\xi(p, q) \equiv p$, $\eta(p, q) \equiv q$ for the boundary value problems (14) and (15) are obtained, so that the initial optimal grid is retained.

6. C-TOPOLOGY GRIDS

At this stage it convenient to describe a set of additional mappings that are necessary to adapt C-topology grids around two-dimensional airfoils; see Fig. 2. The problem is that grid lines of constant $i = i_0$ must be connected to grid lines with $i = IC - i_0$ (IC is the number of cells in the i-direction) if the end points are lying on the wake line, the part of the boundary $j = 0$ which does not belong to the airfoil. Formally the adaption equations can be transformed to the physical domain and the roles of the physical coordinates acting as independent variables and the computational coordinates acting as dependent variables can be interchanged analytically. In this way the branch cut can be treated with complete continuity.

The flow solver, however, that is used in the present paper, based on solution of the Reynolds-averaged Navier–Stokes equations including the Baldwin–Lomax turbulence model, requires that the wake center line coincide with the branch cut and that the grid is orthogonal across the viscous

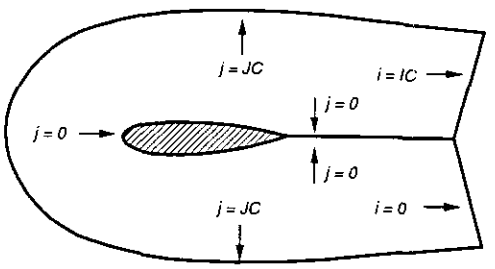

FIG. 2. C-topology around two-dimensional airfoil.

wake. The above-described branch cut treatment does not meet the stated requirements in the viscous wake.

To meet the requirements of both grid continuity and orthogonality across the viscous wake, it is proposed to apply correction mappings such that the initial adaption mapping A is modified minimally. The position of the branch cut is pre-determined by the parametrization of the physical space and could be adapted to the true position of the wake center line. It should be noted that application of correction mappings is a consequence of the flow solver requirements, not a consequence of using a parametric domain.

Two additional correction mappings C^{**} and C^{*} are applied. The mapping C^{**} provides that two grid lines with $i = n_w$ and $i = IC - n_w$, where n_w is the desired number of cells along the wake line, have common end points at the trailing edge of the airfoil. The mapping C^{*} provides common end points along the rest of the wake line. Both mappings are essentially one-dimensional,

$$C^{*}\colon (\xi, \eta) \to (\xi^{*}, \eta), \qquad C^{**}\colon (\xi^{*}, \eta) \to (\xi^{**}, \eta);$$

hence, C^{*} and C^{**} are determined by the functions $\xi^{*}(\xi)$ and $\xi^{**}(\xi^{*})$.

First, the function $\xi^{**}(\xi^{*})$ is taken as

$$\xi^{**} = a_3 \xi^{*3} + a_2 \xi^{*2} + a_1 \xi^{*} + a_0,$$

which minimizes the integral

$$\int_0^1 \left\{ \frac{d^2 \xi^{**}}{d \xi^{*2}} \right\}^2 d\xi^{*}.$$

The constants a_i are determined from four compatibility conditions:

$$\xi^{**}(0) = 0, \qquad \xi^{**}\left(\frac{n_w}{IC}\right) = \xi_{\mathrm{L}}^{**},$$

$$\xi^{**}\left(1 - \frac{n_w}{IC}\right) = \xi_{\mathrm{R}}^{**}, \qquad \xi^{**}(1) = 1,$$

with ξ_L^{**} and ξ_R^{**} implicitly defined by

$$p(\xi_L^{**}) = \frac{n_w}{IC}, \qquad p(\xi_R^{**}) = 1 - \frac{n_w}{IC}.$$

Hence, upon the mere application of C^{**}, i.e., $\xi^* \equiv \xi$, both the lower and upper side of the wake contain n_w cells and the grid lines $i = n_w$ and $i = IC - n_w$ have common end points at the trailing edge.

Second, to obtain grid line continuity over the wake line, the function $\xi^*(\xi)$ is defined on the intervals $0 \leqslant \xi < n_w/IC$ and $1 - n_w/IC < \xi \leqslant 1$ by the implicit equation

$$p(\xi^{**}(\xi^*(\xi))) = \tfrac{1}{2}\{p(\xi^{**}(\xi)) + 1 - p(\xi^{**}(1-\xi))\},$$

where the bracket term represents the mean of the lower and upper grid point distributions along the wake line upon the mere application of C^{**}.

On the remaining interval $n_w/IC \leqslant \xi \leqslant 1 - n_w/IC$, $\xi^*(\xi)$ is taken as

$$\xi^* = b_3\xi^3 + b_2\xi^2 + b_1\xi + b_0,$$

which minimizes the integral

$$\int_{n_w/IC}^{1-n_w/IC} \left\{\frac{d^2\xi^*}{d\xi^2}\right\}^2 d\xi$$

and provides grid smoothness at the trailing edge if the constants b_i are determined from the following compatibility conditions:

$$\xi^*\left(\frac{n_w}{IC}\right) = \frac{n_w}{IC}, \qquad \xi^*\left(1 - \frac{n_w}{IC}\right) = 1 - \frac{n_w}{IC},$$

$$\frac{d\xi^*}{d\xi}\left(\frac{n_w}{IC}\right) = \lim_{\xi \uparrow n_w/IC} \frac{d\xi^*}{d\xi}(\xi),$$

$$\frac{d\xi^*}{d\xi}\left(1 - \frac{n_w}{IC}\right) = \lim_{\xi \downarrow 1 - n_w/IC} \frac{d\xi^2}{d\xi}(\xi).$$

It is easily verified that the application of both C^* and C^{**} yields the properties:

(i) $p(\xi^{**}(\xi^*(n_w/IC))) = n_w/IC$,

(ii) $p(\xi^{**}(\xi^*(1 - n_w/IC))) = 1 - n_w/IC$, and

(iii) $p(\xi^{**}(\xi^*(\xi))) = 1 - p(\xi^{**}(\xi^*(1-\xi)))$
for $0 \leqslant \xi < n_w/IC$ and $1 - n_w/IC < \xi \leqslant 1$,

which ensures common end points at the trailing edge, (i) and (ii), and continuity over the wake line, (iii). The use of the two minimized integrals forces the corrected grid to be very similar to the non-corrected grid.

7. NUMERICAL SOLUTION METHOD

Instead of analytically interchanging the dependent and independent variables of the grid adaption equations (10), which is commonly the method applied in the literature, the boundary value problems (14) and (15) are directly solved for the functions $\xi(p, q)$ and $\eta(p, q)$ which are numerically inverted to the functions $p(\xi, \eta)$ and $q(\xi, \eta)$. An advantage of the present method is that two linear decoupled equations can be solved separately instead of two non-linear coupled equations simultaneously. A disadvantage is the need for an additional computational step to invert the functions $\xi(p, q)$ and $\eta(p, q)$.

Let the initial uniform grid in the parametric domain consist of IC cells in the p-direction and JC cells in the q-direction, where IC and JC are positive integers. The differential operator L_p defined by (12), (13), and (16) can be approximated by a second-order accurate difference operator L_p^h by replacing derivatives by central differences. In an interior grid point ($0 < i < IC$ and $0 < j < JC$) L_p^h is defined as

$$L_p^h[\ ] \equiv \beta_N(\ )_{i,j+1} + \beta_S(\ )_{i,j-1} + \beta_C(\ )_{i,j} + \beta_E(\ )_{i+1,j} + \beta_W(\ )_{i-1,j},$$

with

$$\beta_N = \frac{1}{\Delta q^2}\frac{2\lambda_2^{i,j}}{w_2^{i,j+1} + w_2^{i,j}}, \qquad \beta_S = \frac{1}{\Delta q^2}\frac{2\lambda_2^{i,j}}{w_2^{i,j-1} + w_2^{i,j}},$$

$$\beta_E = \frac{1}{\Delta p^2}\frac{2\lambda_1^{i,j}}{w_1^{i+1,j} + w_1^{i,j}}, \qquad \beta_W = \frac{1}{\Delta p^2}\frac{2\lambda_1^{i,j}}{w_1^{i-1,j} + w_1^{i,j}},$$

$$\beta_C = -(\beta_N + \beta_S + B_E + B_W),$$

where the subscripts and superscripts i, j indicate at which node the functions are evaluated, with $\Delta p = 1/IC$ and $\Delta q = 1/JC$. The normal derivatives at the boundaries of Ω_p are approximated by one-sided differences, e.g.,

$$\frac{\partial}{\partial p}(\ )_{0,j} \approx \frac{1}{\Delta p}\left\{-\frac{3}{2}(\ )_{0,j} + 2(\ )_{1,j} - \frac{1}{2}(\ )_{2,j}\right\},$$

which are also second-order accurate.

Both systems of linear equations that result from the above-described discretizations of the boundary value problems (14) and (15) are solved by red–black Gauss–Seidel relaxation. A correction storage multi-grid technique [15] with fixed V-cycles is used to increase the rate of convergence. No further attention is paid to optimization of the described iteration procedure since this is not the primary goal of the present paper.

The solutions of the above-described linear systems provide values for ξ and η in all points of the uniform grid

in Ω_p and determine the inverse adaption mapping A^{-1} of Fig. 1. The mapping A is determined in discrete form by a set of points $\mathbf{p}_{ij} = (p_{ij}, q_{ij})^T$ that satisfies the following set of algebraic equations:

$$\xi(\mathbf{p}_{ij}) = \left(\frac{i}{IC}, \frac{j}{JC}\right)^T, \qquad i \in [0, IC], \quad j \in [0, JC], \quad (17)$$

where $\xi(\mathbf{p}) = (\xi(\mathbf{p}), \eta(\mathbf{p}))^T$ is a piecewise bilinear interpolation of the points ξ_{ij} and η_{ij}. When Eq. (17) is satisfied, then for all points $(i/IC, j/JC)^T$ of a uniform grid in the computational domain Ω_c associated values of p and q are known, which determines the adaption mapping A. In order to find the set $\mathbf{p}_{ij}$, the following iteration procedure is applied:

$$\mathbf{p}_{ij}^{n+1} = \mathbf{p}_{ij}^{n} - \Delta t \left\{\xi(\mathbf{p}_{ij}^{n}) - \left(\frac{i}{IC}, \frac{j}{JC}\right)^T\right\}. \quad (18)$$

This can be interpreted as an explicit time-stepping scheme with time-step Δt ($\Delta t = 0.1$ in this paper). The stationary solution of (18) satisfies Eq. (17).

Finally the two correction mappings C^* and C^{**} of Section 6 are applied and the obtained adapted grid in the parametric domain Ω_p is mapped to the physical domain Ω by the mapping M; see Fig. 1. At all stages piecewise linear or bilinear interpolation is used to approximate the mappings C^*, C^{**}, A, and M. This concludes the description of the numerical solution method.

8. EXAMPLES OF NUMERICAL GRID ADAPTION

As a first example, the adaption algorithm described in the previous sections is applied to a model problem that simulates the interaction of an oblique shock and a boundary layer represented by a single scalar function $u(x, y)$,

$$u(x, y) = \tanh(10y) - \tanh(5(x-2) - 10y),$$

on the rectangular domain $0 \leqslant x \leqslant 4$, $0 \leqslant y \leqslant 2$. The initial grid of 32×16 cells and a contour plot of the function u are shown in Fig. 3a. Figures 3b–3d show the grid after 1, 2, and 10 adaptions, respectively, where the first adapted grid is taken as the initial grid for the second adaption and so on. The modification functions λ_1 and λ_2 in (10) have been taken as

$$\lambda_1 = \|\mathbf{x}_q\|^2, \qquad \lambda_2 = \|\mathbf{x}_p\|^2.$$

The first adapted grid shows the cell concentration at both the "shock" and the "boundary-layer." The effects of piecewise bilinear interpolation can be observed in the boundary layer and some small wiggles seem to be present which may be caused by even–odd decoupling of the discrete differential equations. These are minor drawbacks, however, and the adapted grid is acceptable. More adaption cycles result in stronger cell concentrations and skew cells at the "shock," but they also show the robustness of the algo-

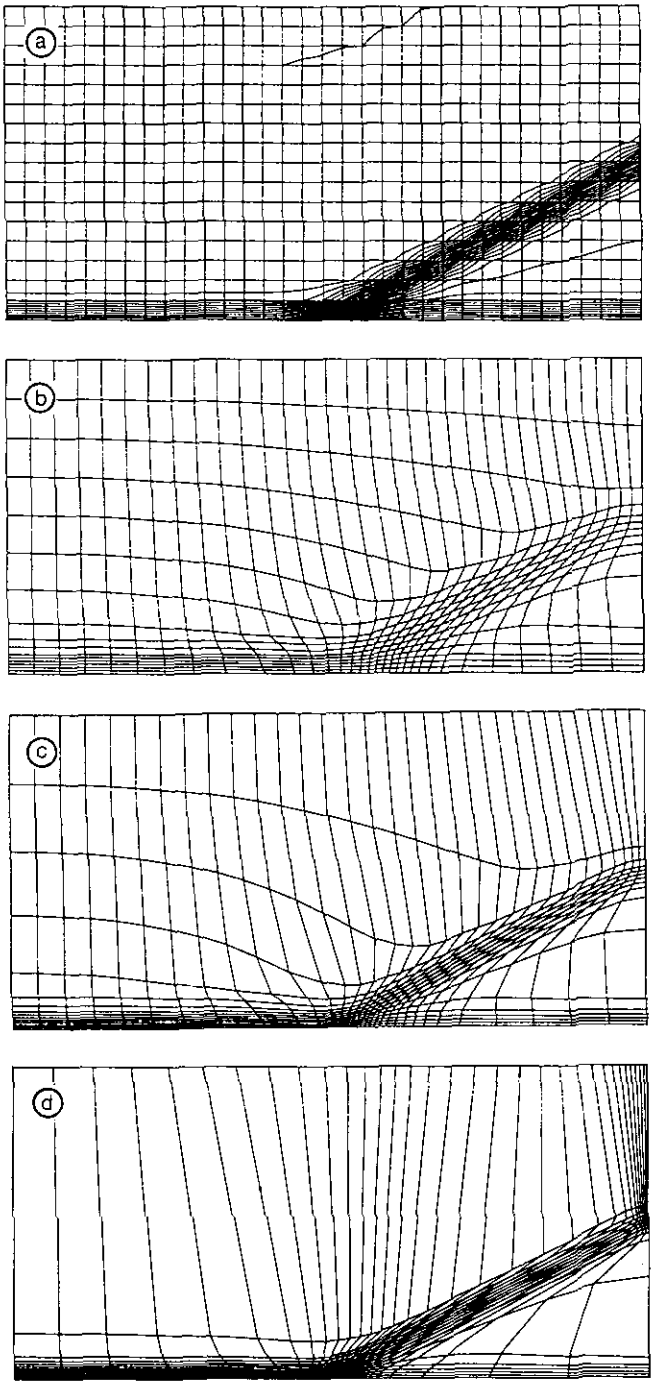

FIG. 3. Initial grid and function contours for oblique-shock/boundary-layer simulation (a), and grids after 1 (b), 2 (c), and 10 (d) adaptions.

rithm since the last adapted grid (Fig. 3d) is still a regular non-overlapping grid.

Figures 4a–4d show the function u in the computational domain initially and after 1, 2, and 10 adaptions, respectively. Already after one adaption the gradients in the computational domain decrease significantly, and after 10 adaptions the "shock" and "boundary layer" almost disappear. Finally it may be noted that the first adaption is the most effective one; see Figs. 4a–4b, while the following adaptions show less rigorous effects.

The next example shows the influence of the modification functions λ_1 and λ_2 in (10) on the adaption of a highly stretched grid around the leading edge of an airfoil, see Figs. 5a–5e. When $\lambda_1 \equiv \lambda_2 \equiv 1$, see Fig. 5b, the adapted grid is excessively skew in and near the boundary layer, which is in agreement with the analysis of Section 4.

When $\lambda_1 = \|\mathbf{x}_q\|$, $\lambda_2 = \|\mathbf{x}_p\|$ (see Fig. 5c), the adapted grid outside the boundary layer has improved significantly; however, inside the boundary layer (not shown) the grid is still skew. When $\lambda_1 = \|\mathbf{x}_q\|^2$, $\lambda_2 = \|\mathbf{x}_p\|^2$ (see Fig. 5d) the adapted grid is also orthogonal in the boundary layer (not shown) while the grid adaption in the normal direction to the airfoil surface dominates. But this unfortunately results in excessive depletion of cells in the tangential direction; compare Figs. 5a, 5b, and 5d. In order to obtain both one-dimensional equidistribution in the normal direction inside the boundary layer and adaption in the tangential direction controlled by the flow at the edge of the boundary layer, the following choice for the modification functions is proposed:

$$\lambda_1 = w_1^2 \|\mathbf{x}_q\|^2, \qquad \lambda_2 = w_2^2 \|\mathbf{x}_p\|^2. \tag{19}$$

Because just outside the boundary layer flow-solution derivatives in the normal direction are much smaller than in the tangential direction ($w_2 \ll w_1$), the tangential adaption dominates when $\|\mathbf{x}_q\|/\|\mathbf{x}_p\|$ is not too small. The resulting

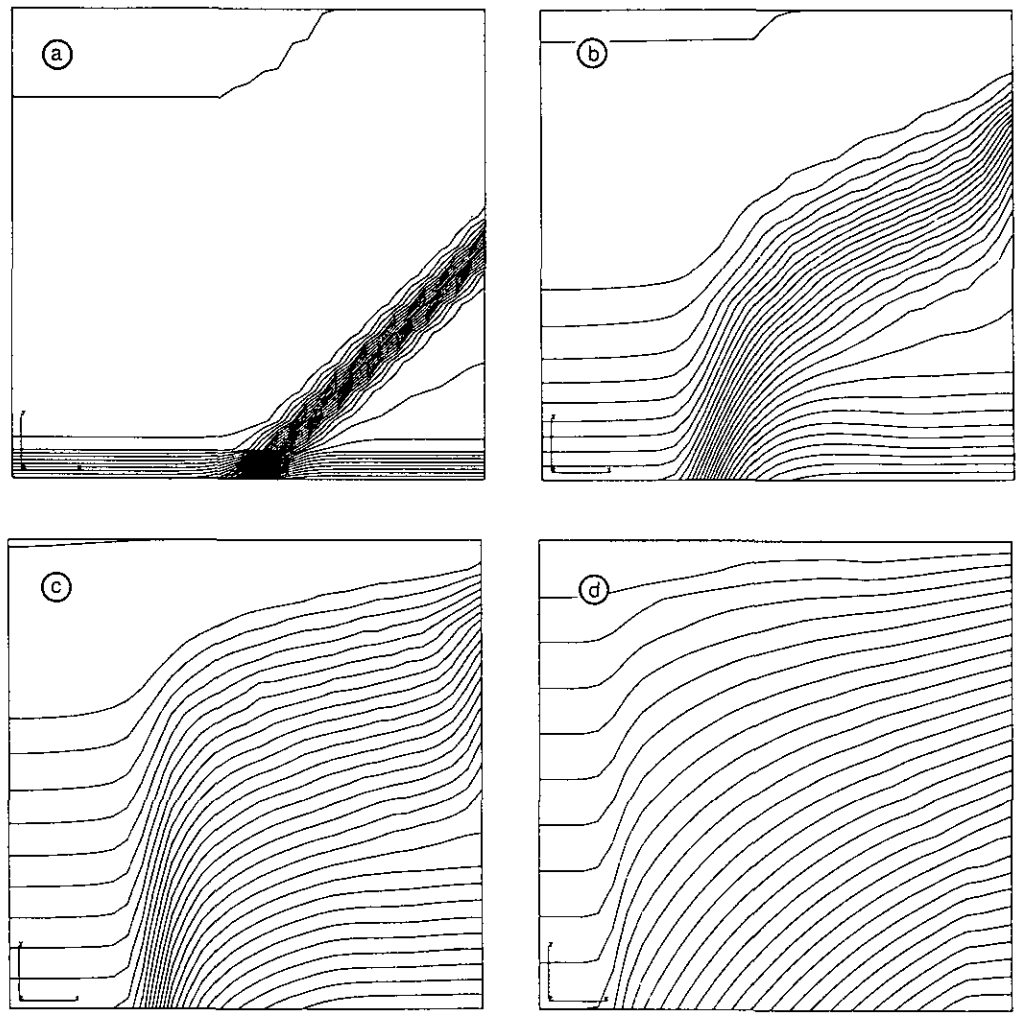

FIG. 4. Function contours in the computational domain for oblique-shock/boundary-layer simulation: initially (a) and after 1 (b), 2 (c), and 10 (d) adaptions.

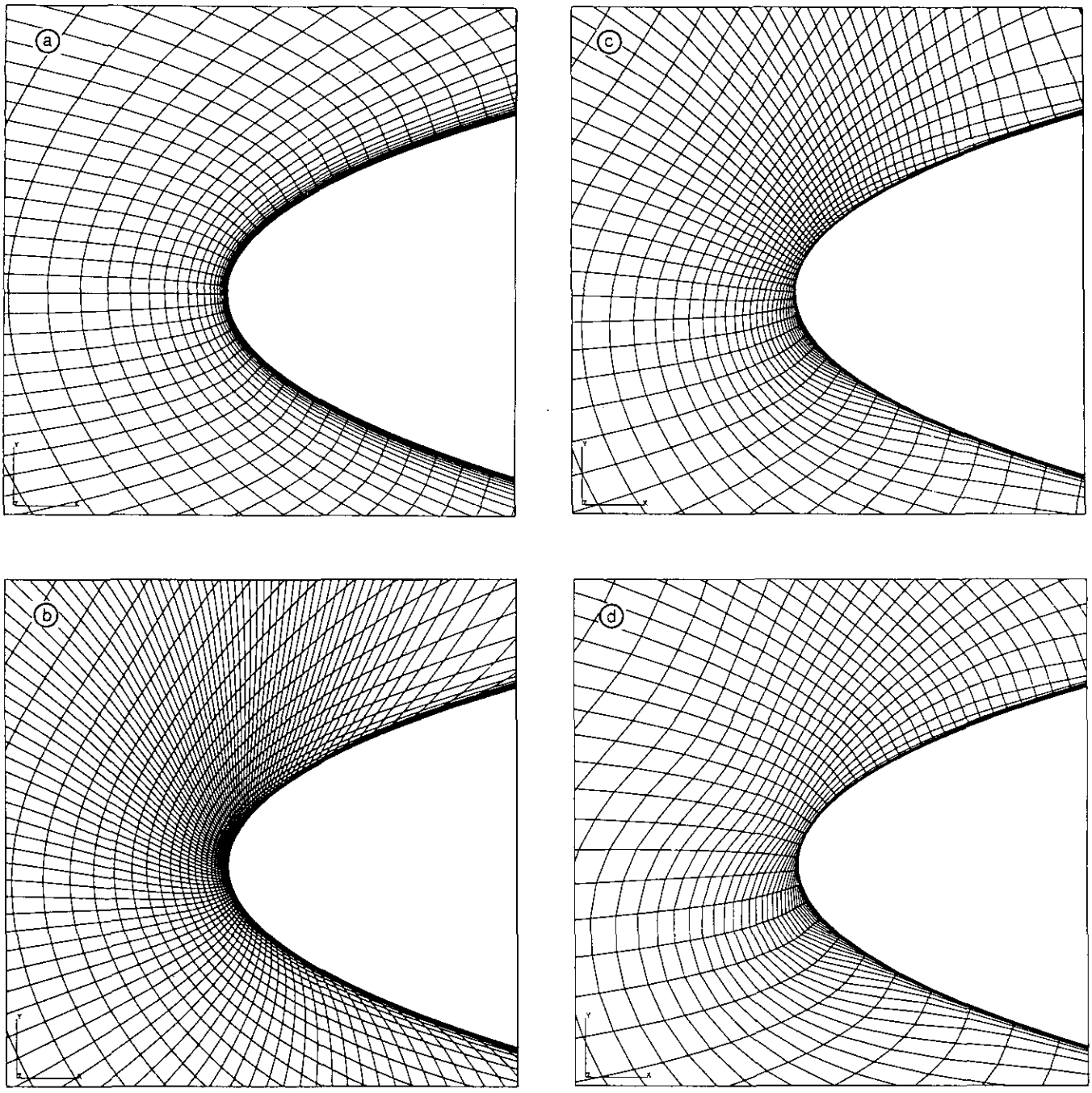

FIG. 5. Initial grid (a) and adapted grid (b) around leading edge with $\lambda_1 \equiv \lambda_2 \equiv 1$. Adapted grid around leading edge with $\lambda_1 = \|\mathbf{x}_q\|$, $\lambda_2 = \|\mathbf{x}_p\|$ (c), with $\lambda_1 = \|\mathbf{x}_q\|^2$, $\lambda_2 = \|\mathbf{x}_p\|^2$ (d), with $\lambda_1 = w_1^2 \|\mathbf{x}_q\|^2$, $\lambda_2 = w_2^2 \|\mathbf{x}_p\|^2$ (e), and close-up of the upper side (f).

adapted grid is depicted in Fig. 5e, which shows that grid lines in the normal direction to the airfoil enter the boundary layer orthogonally while around the leading edge the grid is also significantly refined w.r.t. the initial grid. Inside the boundary layer the grid is also orthogonal, see Fig. 5f. Hence, the choice (19) for the modification functions is used in the remainder of this section.

The final example consists of the adaption of a C-topology grid around the RAE 2822 airfoil suitable for solution of the Reynolds-averaged Navier–Stokes equations ($M_\infty = 0.7250$, $\mathrm{Re}_\infty = 6.5 \times 10^6$, $\alpha = 2.44°$). The grid consists of 352×64 cells with 256 cells along the airfoil, 48 cells at both sides of the wake line, and 64 cells in the normal direction to both the airfoil and the wake line. The flow

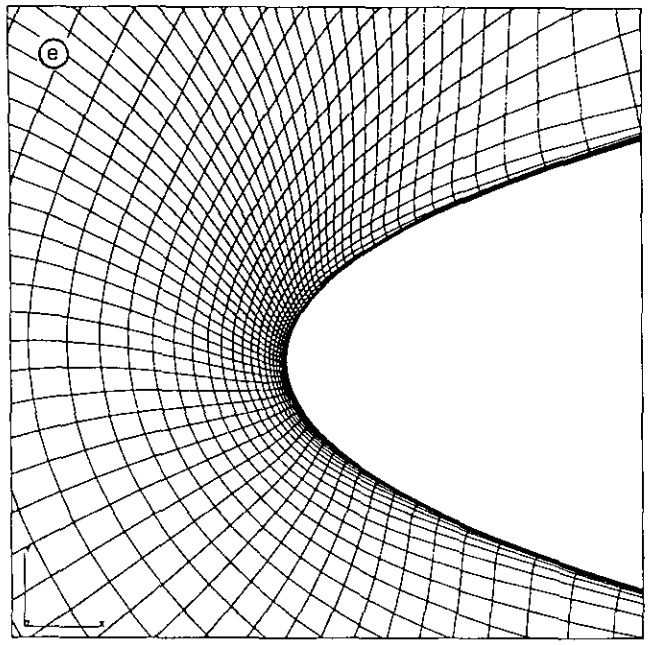

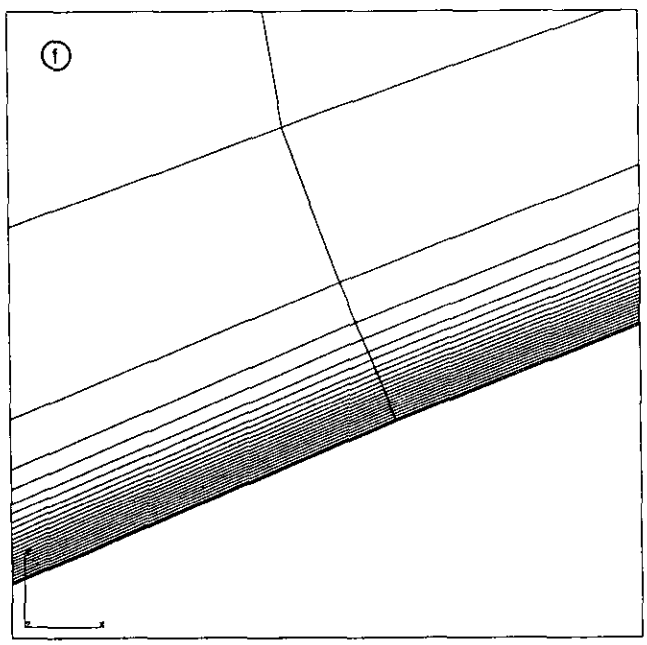

FIG. 5—*Continued*

equations are solved with a vertex-based central-difference scheme combined with the Baldwin–Lomax turbulence model, described by Brandsma [16]. Large parts of the initial and adapted grids are shown in Figs. 6a–6b and detailed views are depicted in Figs. 5a, 5e (leading edge area) and in Figs. 7a, 7b (shock area). The weight functions have been smoothed three times as

$$w_{ij}^{k} = \tfrac{1}{2} w_{ij}^{k-1} + \tfrac{1}{16} \{ w_{i-1j+1}^{k-1} + w_{ij+1}^{k-1} + w_{i+1j+1}^{k-1} + w_{i-1j}^{k-1} + w_{i+1j}^{k-1} + w_{i-1j-1}^{k-1} + w_{ij-1}^{k-1} + w_{i+1j-1}^{k-1} \},$$

to eliminate spurious oscillations. The execution time needed to solve the adaption equations and to invert the adaption mapping amounts about 75 CPU seconds on a NEC SX-3 supercomputer, needed for 1254 V-cycles on the

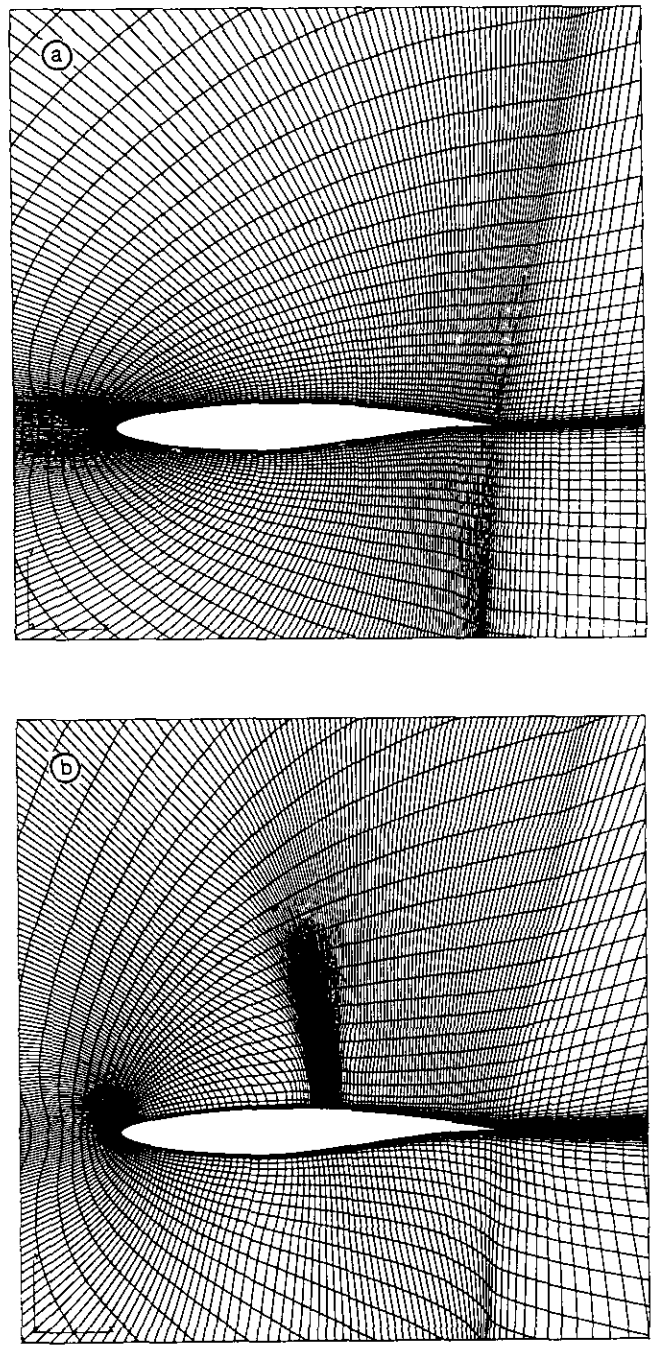

FIG. 6. Initial (a) and adapted (b) grids around RAE2822 airfoil for transonic flow conditions ($M = 0.725$, $\mathrm{Re} = 6.5 \times 10^6$, $\alpha = 2.44°$).

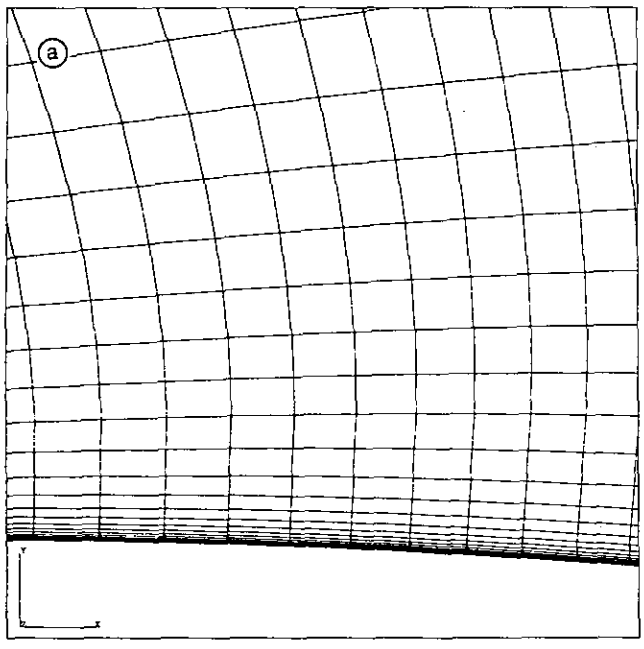

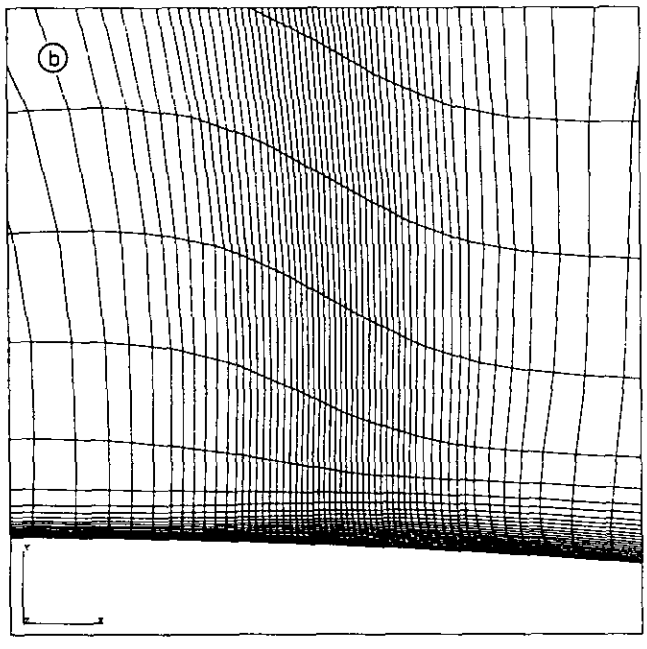

FIG. 7. Initial (a) and adapted (b) grids at the shock region.

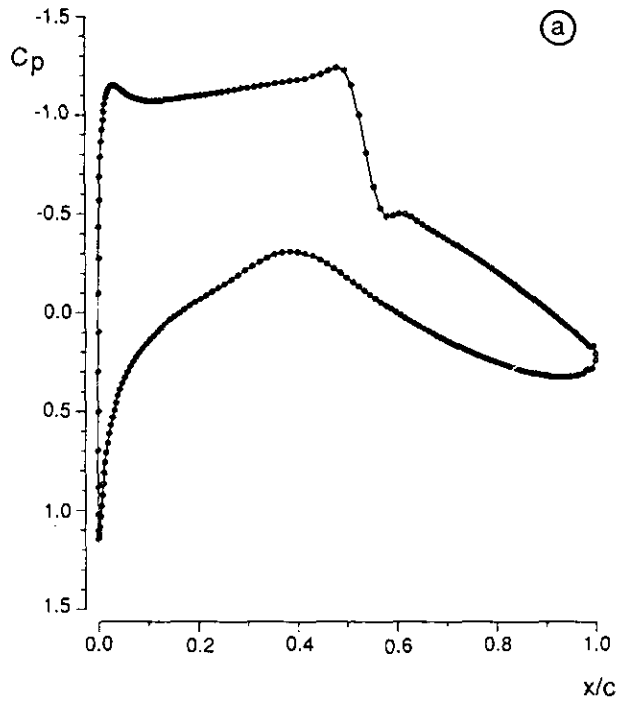

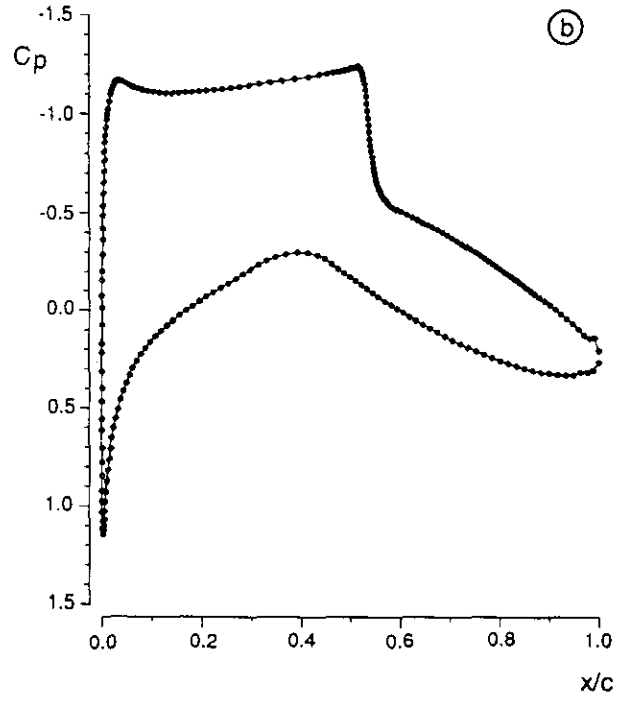

FIG. 8. Pressure distributions along the airfoil calculated on the initial (a) and adapted (b) grids.

ξ-equation, 974 V-cycles on the η-equation, and 961 iterations on the inversion equations to decrease the maximum residuals 11, 12, and 14 orders of magnitude, respectively.

The pressure distributions along the airfoil surface are shown in Figs. 8a, 8b, and the Mach number contours are shown in Figs. 9a, 9b. Both the shock and the leading edge expansion are better resolved on the adapted grid. Behind the shock the kink in the pressure distribution has disappeared and the Mach number distribution just outside the boundary layer has become more uniform in the normal direction. The lift coefficient changed from 0.7714 to 0.7926 (2.7%), the drag coefficient changed from 0.01259 to

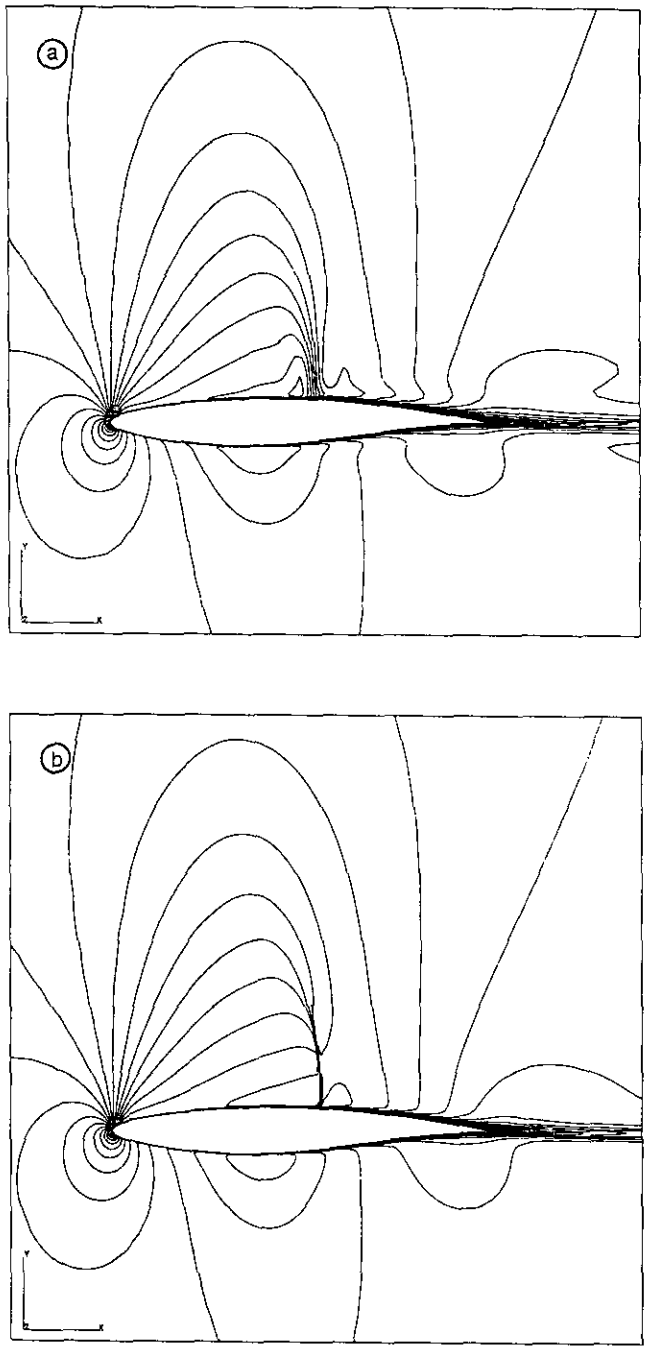

FIG. 9. Mach number distributions calculated on the initial (a) and adapted (b) grids.

0.01248 (1 count) and the pitching coefficient changed from -0.09125 to -0.09399 (3%).

Finally it is interesting to see how the flow solution in the computational domain changed due to grid adaption and recalculation of the flow. In Figs. 10a–10b the Mach number distribution is depicted in the computational domain. Both the expansion zone at the leading edge and the boundary layer are more smoothly distributed in the adapted case (Fig. 10b). The shock in the boundary layer has smeared out and the shock in the inviscid outer flow has been regenerated by recalculation of the flow. An exception is the trailing edge region, where gradients in the computational domain are increased upon grid adaption in the lowest part of the boundary layer. This is probably caused by the modification function λ_1 defined in (19) which is less sensitive for gradients in the streamwise direction when the initial grid has locally very high aspect ratios. In Figs. 11a–11b the pressure-coefficient distribution is

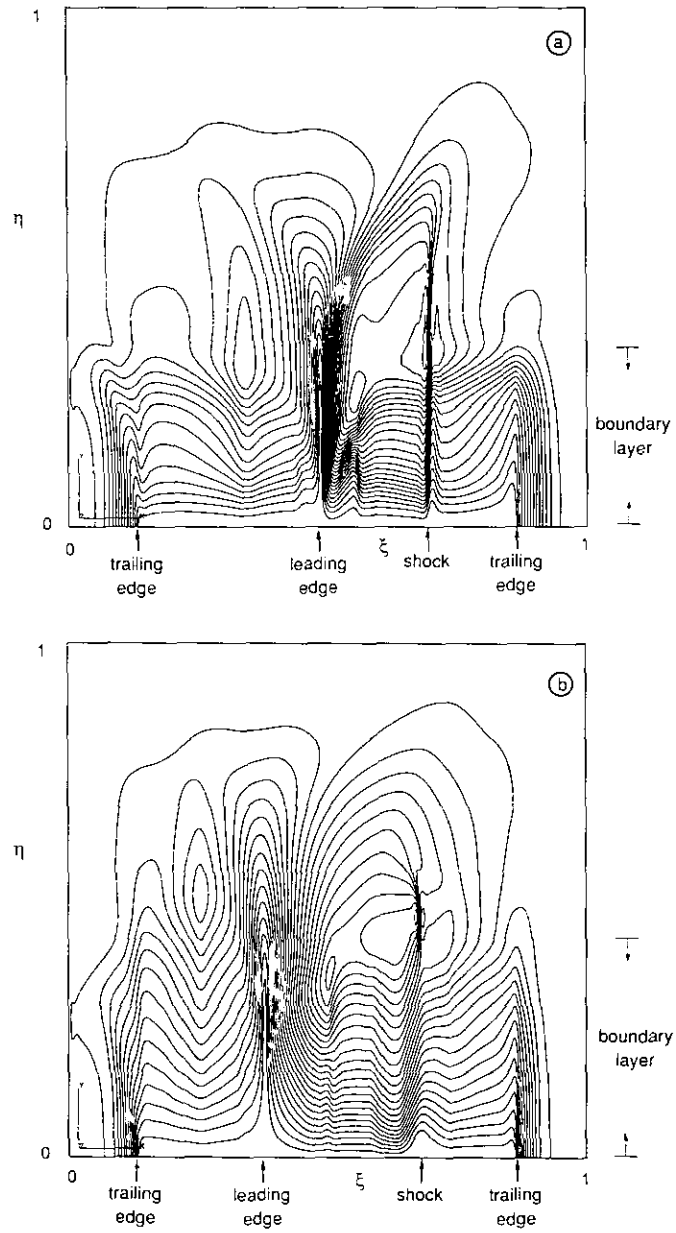

FIG. 10. Mach number distributions in the computational domain calculated on the initial (a) and adapted (b) grids.

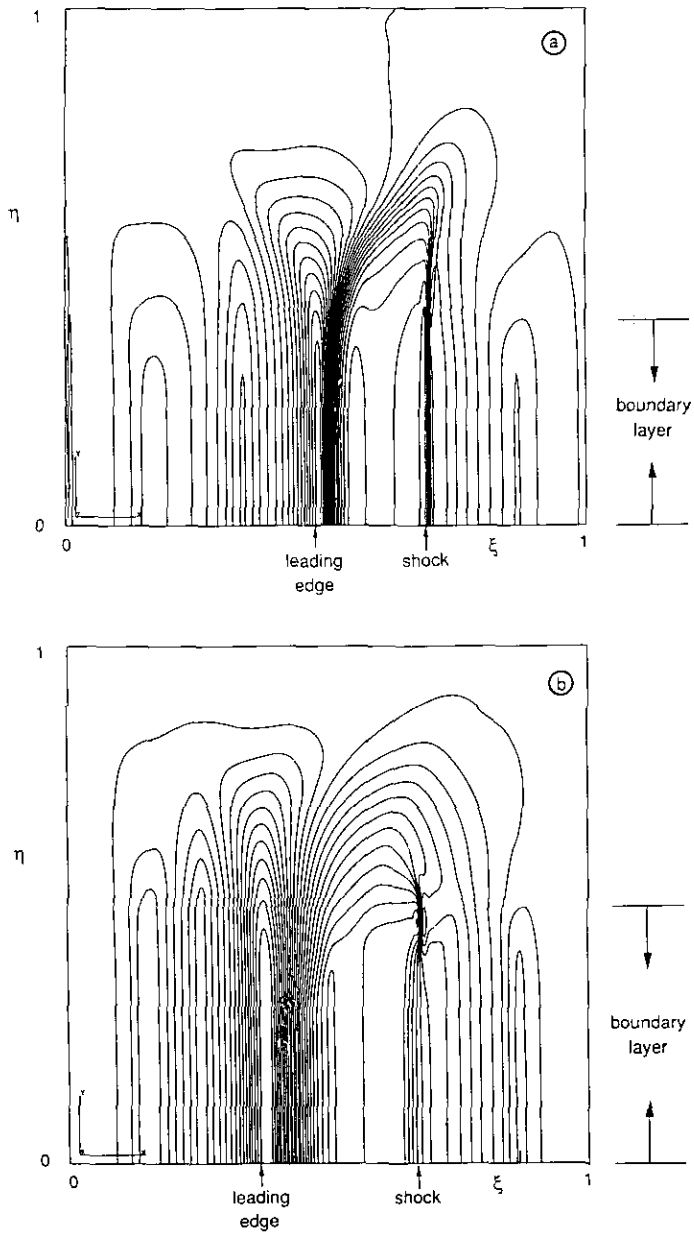

FIG. 11. Pressure coefficient distributions in the computational domain calculated on the initial (a) and adapted (b) grids.

depicted in the computational domain. The same effects as for the Mach number distribution can be observed. This concludes the description of grid adaption examples.

9. CONCLUSIONS

A new grid adaption algorithm for computational fluid dynamics problems in two space dimensions has been developed. Four essential steps in the algorithm can be distinguished:

(i) The adapted equations are formulated in the so-called parametric domain associated with the initial grid that has to be adapted.

(ii) The basic adaption equations are derived from variational principles and can be interpreted as anisotropic diffusion equations.

(iii) The adaption equations are modified to obtain the following desirable properties in boundary layers:

— preservation of orthogonality,

— one-dimensional equidistribution of a weight function in the normal direction, and

— adaption in the flow direction controlled by the outer flow.

(iv) The modified anisotropic diffusion equations are directly solved for the computational coordinates (ξ, η) as functions of the parametric coordinates (p, q) and the resulting mapping is numerically inverted.

The functional that is minimized to give the anisotropic diffusion equations mentioned under (ii) can be interpreted as the sum of weighted norms of tangents along curves of constant p or q in the computational domain. This is different from the functionals of Winslow [9] and Eiseman [1], which can be interpreted as the sum of weighted norms of normals to curves of constant ξ and η in the parametrical or physical domain.

The present algorithm appears to be robust in the sense that for the presented adaption examples no overlapping cells are generated while the initial grids are heavily adapted. A model problem for oblique-shock/boundary-layer simulation characterized by a scalar function u shows that upon 10 successive adaption cycles the function u tends towards a very smooth distribution in the computational domain. The same effect can be observed to some extent from a second numerical example, where both the Mach number and the pressure-coefficient distribution associated with the flow around the RAE2822 airfoil become globally smooth functions in the computational domain upon grid adaption and recalculation of the flow solution. This is considered as a positive feature of the adaption algorithm because numerical errors in the flow solution can partly be traced back to second derivatives of the flow solution in the computational domain. The Navier–Stokes test case also shows that the shock and boundary layer are well resolved on the adapted grid and that the grid is orthogonal throughout the entire boundary layer and wake. For C-topology grids it is essentially necessary to apply additional correction mappings to provide common end points of grid lines at the trailing edge and grid continuity across the wake line. The present construction of the correction mappings is based on two minimization problems; this ensures that the characteristics of the initially adapted grid are globally retained.

In conclusion it is stated that the present grid-adaption algorithm is promising w.r.t. robustness and boundary-layer properties. The possible occurrence and drawback of grid skewness, as well as the influence of grid adaption in successive parametric domains are issues to be analyzed in future work.

ACKNOWLEDGMENTS

The author thanks Dr. B. Oskam for reading the manuscript carefully and giving many suggestions that contributed to improvement of the work and K. M. J. de Cock for many fruitful discussions and comments and for developing several subroutines that have extensively been used during the work.

REFERENCES

1. P. R. Eiseman, *Computer Methods Appl. Mech. Engrg.* **64**, 321 (1987).
2. J. F. Thompson, AIAA-84-1606, Snowmass, CO, June 1984 (unpublished).
3. H. A. Dwyer, *AIAA J.* **22** (12), 1705 (1984).
4. K. Nakahashi and G. S. Deiwert, *AIAA J.* **24** (6) 948 (1986).
5. D. A. Anderson and J. Steinbrenner, AIAA-86-0427, Reno, NV, January 1986 (unpublished).
6. D. A. Anderson, *Appl. Math. Comput.* **24**, 211 (1987).
7. J. F. Thompson, F. C. Thames, and C. M. Mastin, *J. Comput. Phys.* **15**, 299 (1974).
8. D. A. Anderson, AIAA-87-0202, Reno, NV, January 1987 (unpublished).
9. A. Winslow, UCID-19062, Lawrence Livermore National Laboratories, University of California, 1981 (unpublished).
10. K. D. Lee and J. M. Loellbach, AIAA-89-2178, Seattle, WA, July 1989 (unpublished).
11. J. U. Brackbill and J. S. Saltzman, *J. Comput. Phys.* **46**, 342 (1982).
12. Z. U. A. Warsi and J. F. Thompson, *Comput. Math. Appl.* **19** (8/9), 31 (1990).
13. H. J. Kim and J. Thompson, AIAA-88-0311, Reno, NV, January 1988 (unpublished).
14. R. Courant and D. Hilbert, *Methods of Mathematical Physics*, Vol. I (Wiley, New York, 1989).
15. A. Brandt, *Math. Comp.* **31** (138), 333 (1977).
16. F. J. Brandsma, "Description of the Method Used by NLR," *EUROVAL—A European Initiative on Validation of CFD Codes*, edited by W. Haase *et al.* Notes on Numerical Fluid Mechanics, Vol. 42 (Vieweg, Brunswick, 1993).